Colloid Polym Sci 278:547–552 (2000)

ORIGINAL CONTRIBUTION

B. Traub
T. Fritzhanns
S. Hafner
H. W. Spiess

Characterization of superabsorbing polymers by NMR imaging

Received: 2 November 1999
Accepted: 17 December 1999

B. Traub · T. Fritzhanns · S. Hafner
H. W. Spiess (✉)
Max-Planck-Institut für Polymerforschung
Postfach 3148, 55021 Mainz, Germany
e-mail: spiess@mpip-mainz.mpg.de
Tel.: +49-6131-379121
Fax: +49-6131-379100

Abstract The use of NMR imaging techniques for the characterization of superabsorbing polymers is explored. Spatial differences in the cross-link densities of polyacrylate-based superabsorbing particles are investigated by parameter-selective ^{1}H NMR imaging of samples swollen with water. Images of the transverse relaxation time and of the self-diffusion coefficient of the absorbed water provide valuable information on the local water mobility and, thus, indirectly also on the polymer. The time evolution of the swelling process was also studied by NMR images acquired after different swelling times. Moreover, using magic-angle-spinning imaging, the influence of mechanical load on the swollen particle was investigated by taking advantage of the centrifugal forces on the spinning sample. These experiments indicate the presence of two water components, one strongly adsorbed, while the other is relatively mobile.

Key words Polyacrylate · Super absorber · Diffusion NMR imaging

Introduction

Superabsorbing polymers (SAPs) are nowadays widely used in many parts of life. They usually consist of network structures of acrylic acid polymerized in the presence of its salts. The resulting product can absorb up to 100 times more water than its own weight, which makes it an important component of personal hygiene products. However, although 95% of the overall world production of 900,000 t is presently used for the production of diapers, there is also an increasing number of other applications. Superabsorbers are used for the sealing of the Channel Tunnel between England and France [1], the protection of underwater fiberglass cables, the moistening of warehouses, as a basis for the production of artificial snow [2] and for many other purposes. An overview of these and other applications can be found in Ref. [3]. For this wide applicability in many product areas, superabsorbing polymers have become a major research topic in the polymer industry and there is great interest in new characterization techniques that provide the basis for future improvements of these materials.

One such characterization method that has become more and more powerful in recent years is NMR imaging. This technique, nowadays already an indispensable diagnostic tool in medicine, also provides interesting possibilities for the characterization of materials [4–8]. It is nondestructive and allows spatially resolved NMR spectroscopic parameters to be acquired, to name the two most important advantages. That is, microscopic and macroscopic properties of a material can be conveniently correlated.

In this article we explore the use of this promising method for the characterization of spatially varying material properties in SAPs that are not so easily accessible by other methods. We investigate the properties of the sample indirectly by the imaging of water in swollen SAPs. From images of suitable parameters that are directly related to the mobility of the absorbed water we draw conclusions on the corresponding properties of the super absorber. Such indirect investigations of material properties by the imaging of a solvent often provide more useful information than the direct imaging of the material itself [8–11].

Experimental

The NMR imaging experiments were performed on a Bruker MSL-300 NMR spectrometer equipped with imaging facilities. The B_0 field of 7.05 T corresponds to a ^{1}H resonance frequency of 300 MHz. For the conventional imaging experiments, a commercial Bruker microimaging probe head was used with a 5 mm (internal diameter) radio-frequency (RF) saddle coil. The 90° pulse length was set to 4 μs and the RF inhomogeneity was found to be negligible over the sample (which was about 1 mm in diameter). The magic-angle-spinning (MAS) imaging experiments described later were performed with a homebuilt probe.

Standard 2D spin-echo imaging sequences were applied instead of fast-imaging techniques based on gradient echoes in order to suppress possible effects of field inhomogeneities and susceptibility. Both, Fourier and back-projection techniques were used for image reconstruction. The pulse sequence for the Fourier spin-echo technique is shown in Fig. 1 as an example. Spatial resolution of better than 50 μm in 2D is provided by a phase-encoding gradient of strength 48.3 G/cm and a frequency encoding gradient of 14.6 G/cm. In case of back-projection imaging, a read gradient of 13.7 G/cm is rotated in 120 steps from 0 to 180 degrees and the image is reconstructed from the resulting profiles. No slice selection is applied for signal-to-noise reasons, so the NMR parameters discussed later represent an average over the third dimension.

In order to probe the mobility of the water inside the swollen SAPs, suitable NMR parameters had to be chosen first [12]. The transverse relaxation time, T_2, and the water diffusion coefficient were found to be sensitive parameters for our purpose. For the measurement of the first, the time, t_E between the 90° pulse and the 180° pulse was varied in successive imaging experiments so that a series of T_2-weighted images was acquired. From this series, a spin-density image and a T_2-parameter image can be evaluated. For the evaluation of T_2, the (normalized) decay of the signal for each spatial coordinate was fitted with the exponential function

$$S(r,t) = A(r) + B(r)\exp[-t/T_2(r)]$$

where $B(r)$ denotes the local signal amplitude, $T_2(r)$ characterizes the local relaxation time and $A(r)$ accounts for a possible constant signal offset which, however, was found to be negligible, i.e., $A(r) = 0$. As a result of the fitting, two parameter maps are obtained, one representing the spin-density image, $B(r)$, and the other the image of the transverse relaxation time, $T_2(r)$.

The diffusion-imaging experiment was performed with the pulse sequence shown in Fig. 2 [13–14], where the spin-echo sequence is replaced by a stimulated-echo sequence to allow longer diffusion times to be used. In order to measure the diffusion coefficient, two magnetic-field gradient pulses in the z direction were applied for a time, δ, in addition to the imaging gradients in the x and y directions. The two z-gradient pulses were separated by the time Δ and their strength, g, was varied between 0 and 24 G/cm. For a fixed value of g, a diffusion-weighted NMR image is obtained that provides qualitative information on the diffusion along the z direction. By systematically changing the strength of the diffusion gradients, a series of such z-diffusion-weighted images can be acquired.

For the evaluation of this series, the diffusion decay was fitted for each spatial coordinate with the Stejskal–Tanner relation [15],

$$S(r,t) = A(r) + B(r)\exp[-\gamma^2 g^2 \beta D(r)] \ ,$$

with $\beta = \delta^2(\Delta - \delta/3)$. $D(r)$ denotes the local self-diffusion coefficient, γ is the magnetogyric ratio and the times δ and Δ are indicated in Fig. 2. $B(r)$ is the local amplitude of the exponential decay, i.e. the local spin density attenuated by T_2 relaxation and by additional diffusion weighting due to the x read gradient (which is of the same order of magnitude as that provided by the diffusion gradient). The diffusion decay is acquired by varying the gradient strength and two parameter maps are obtained by the corresponding fits representing $B(r)$ and, much more interesting, the self-diffusion-coefficient image, $D(r)$.

In all static experiments, a sampling time (dwell time) of 5 μs was used and 128 data points were acquired for each projection or phase-encoding step, respectively. From the resulting data sets, a 128×128 pixel image was constructed. Since the water line was sufficiently narrow, the resolution was limited in all experiments by the pixel resolution of about 40 μm. The data analysis and presentation was performed with the PV-Wave software package (Visual Numerics) running on a DEC 3000 alpha workstation.

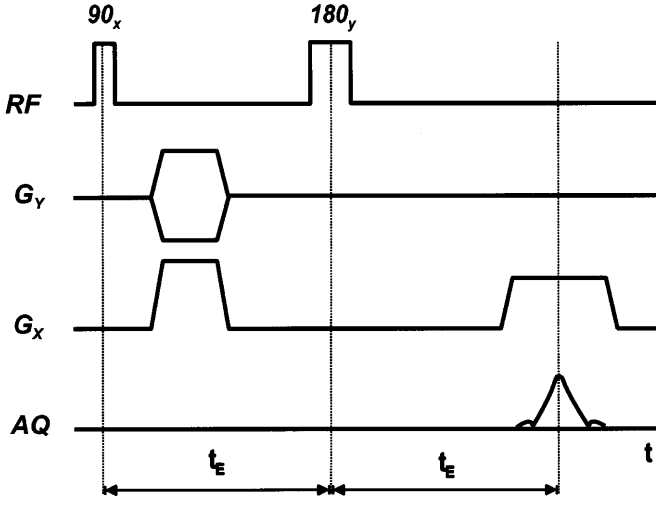

Fig. 1 Standard 2D Fourier spin-echo imaging scheme used for the acquisition of the T_2-relaxation-time images. The time t_E is varied in a series of successive experiments. From the resulting relaxation-weighted images, a T_2 image can be calculated

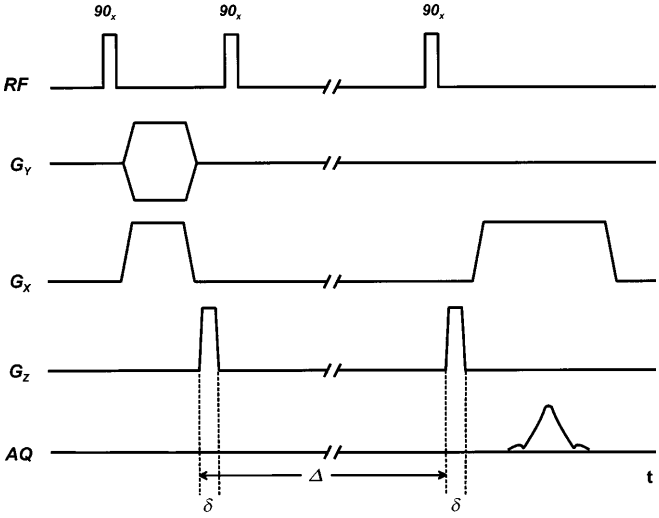

Fig. 2 Stimulated-echo imaging sequence for the acquisition of self-diffusion-constant images. The gradients in the x and y directions are used for the imaging, while G_z represents the diffusion gradient. Systematic incrementation of the diffusion gradient provides a series of self-diffusion-weighted images from which the self-diffusion-constant image can be evaluated

In order to investigate the sample under mechanical load, MAS imaging was also applied [16–18]. In such MAS experiments, the sample is spun rapidly around an axis aligned at the so-called magic angle with respect to the magnetic field. For this angle, the anisotropic spin interactions vanish. The technique, therefore, is usually applied for line-narrowing in solid-state NMR spectroscopy and, more recently, it has also been exploited for the imaging of solids. In the case of swollen SAPs, however, the ^{1}H NMR lines are sufficiently narrow, so additional line-narrowing is not required. The only motivation for the use of MAS on our samples is to simulate mechanical load by taking advantage of the centrifugal forces on the spinning sample.

The imaging pulse sequences used under MAS conditions are similar to those described earlier. The equipment for these experiments, however, is nonstandard and highly sophisticated since it involves the generation of gradients that rotate synchronously with the spinning sample. Details of the instrumentation can be found in Refs. [17, 18].

The samples used in all experiments were commercial polyacrylate-based SAPs that have been additionally cross-linked after reduction to small pieces to improve the mechanical properties. This additional cross-linking of the surface is nowadays a standard procedure in the production process. The SAPs were prepared for the imaging experiment as follows. For the images in Figs. 3 and 4, one SAP particle was swollen in water for 24 h, after which it is guaranteed that it has reached the fully swollen state. Gravimetric measurements show that the sample then consists of more than 95% water, so nearly all the signal intensity in the images will originate from water. For investigating the swelling as a function of time, the SAPs were brought into contact with water for the corresponding time directly before the imaging experiment. For MAS imaging, the SAP samples were swollen with water until the weight ratio was 1:1 and were then put in a 7-mm Bruker MAS rotor.

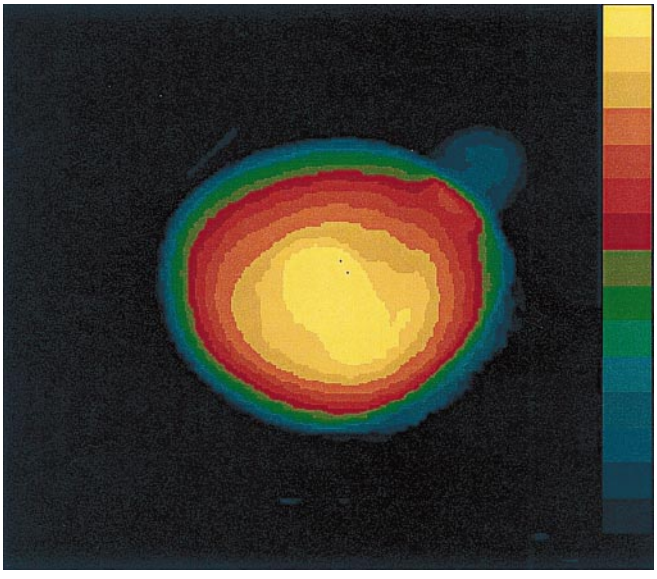

Fig. 3 T_2-relaxation-time image of water in a fully swollen superabsorbing particle (the *color scale* corresponds to a T_2 range between 0 and 8 ms). The difference in T_2 between the inner and outer parts of the particle is clearly visible. A more detailed discussion can be found in the text

Results

As already mentioned, the SAPs were additionally cross-linked in the outer parts. Apart from that, undesired cross-linking inhomogeneities might also be present in the inner parts. In order to visualize these effects, water was used as a probe and it was assumed that the average mobility of the water molecules in the SAPs changed corresponding to the mobility and structure of the network in close proximity.

The T_2-parameter image of an individual swollen SAP acquired using the back-projection technique is shown in Fig. 3. The particle is not fully rotationally symmetric, for instance, there is a small appendage in the upper right part and also the region of highest T_2 values is shifted somewhat towards the bottom of the image. The image clearly shows that the relaxation times of the water in the inner parts of the particle are longer than in the outer regions, i.e., $T_2 = 8$ ms is found in the central part, while in the outer parts $T_2 = 3$ ms. This might be interpreted in terms of the greater mobility of the water molecules in the inner parts, since the transverse relaxation time is sensitive to translational and rotational motions taking place on a nanometer scale. This finding is a direct hint for the change in the cross-link density discussed earlier and demonstrates that the T_2 value of the absorbed water is indeed sensitive to these changes in the material.

The swelling process of one SAP is shown for five swelling times in Fig. 5. For this, the particle was swollen for different times and imaged immediately after the swelling using a 2D Fourier transform spin-echo sequence. In the upper part of Fig. 5, the spin-density images of the SAP are shown after swelling for 30 s, 3 min, 5 min, 10 min and 30 min, respectively. The corresponding T_2 images are displayed in the lower part of the image. The images in Fig. 5 show an increase in size due to swelling between the first and the second image. After this, not much change in size is observed (note that the orientation of the sample with respect to the imaging plane is different in the five image pairs). As in the T_2 image of the particles fully swollen discussed earlier, all T_2 images of the series show a shorter relaxation time in the outer shell, corresponding to reduced water mobility throughout the swelling process. Moreover, they show some structural details which, however, cannot be interpreted in terms of different swelling times since the orientation of the image plane is different for the different images.

The 2D Fourier transform image of the self-diffusion coefficient of the fully swollen SAP discussed already in connection with Fig. 3 is shown in Fig. 4. The difference in shape compared to the T_2 back-projection image is due to the difference in sample orientation with respect to the imaging plane and to the reduced resolution in the

outer parts of the back-projection image (Fig. 3) as is characteristic for this technique.

Nevertheless, like the T_2 image, the diffusion image also shows differences between the outer and inner regions of the sample. While in the inner region one finds a self-diffusion constant of about 5×10^{-4} mm^2/s, the constant is reduced to about 2.5×10^{-4} mm^2/s in the outer parts of the sample, again reflecting structural differences in the two regions. The thickness of the outer region with a higher network density is about 150 ± 50 μm in the fully swollen state.

As in the T_2 image, the inner region of higher mobility is shifted somewhat off-center (here the sample is oriented such that this region is in the upper part of the image), but now more structural details are also revealed. This might be mainly due to the different length scales probed by diffusion and transverse relaxation. In contrast to T_2, which probes local dynamics on the molecular level, the diffusion coefficient probes the translative mobility of the water in the direction of the applied diffusion gradient (here z direction). It is sensitive to motions taking place on a much longer length scale as in the case of T_2, i.e., in the micron range. The parameter image of the diffusion constant thus reveals local inhomogeneities of the network on a larger length scale.

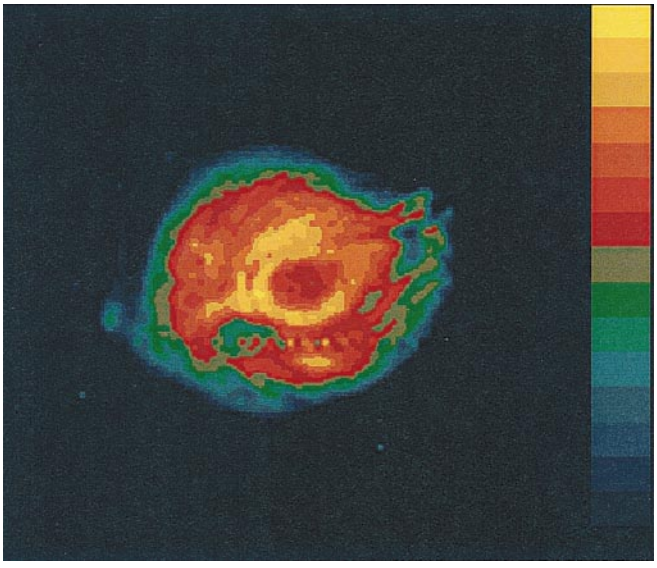

Fig. 4 Self-diffusion-constant image of a fully swollen superabsorbing particle again showing a difference in the water mobility in the inner and outer regions. Self-diffusion measurements are sensitive to translational motions on a micron scale. The corresponding image also reveals structural details within the inner region of the sample. The *color scale* represents values between $D = 2 \times 10^{-4}$ mm^2/s and 6×10^{-4} mm^2/s

Finally, the SAP was investigated under mechanical load provided by the centrifugal forces during MAS

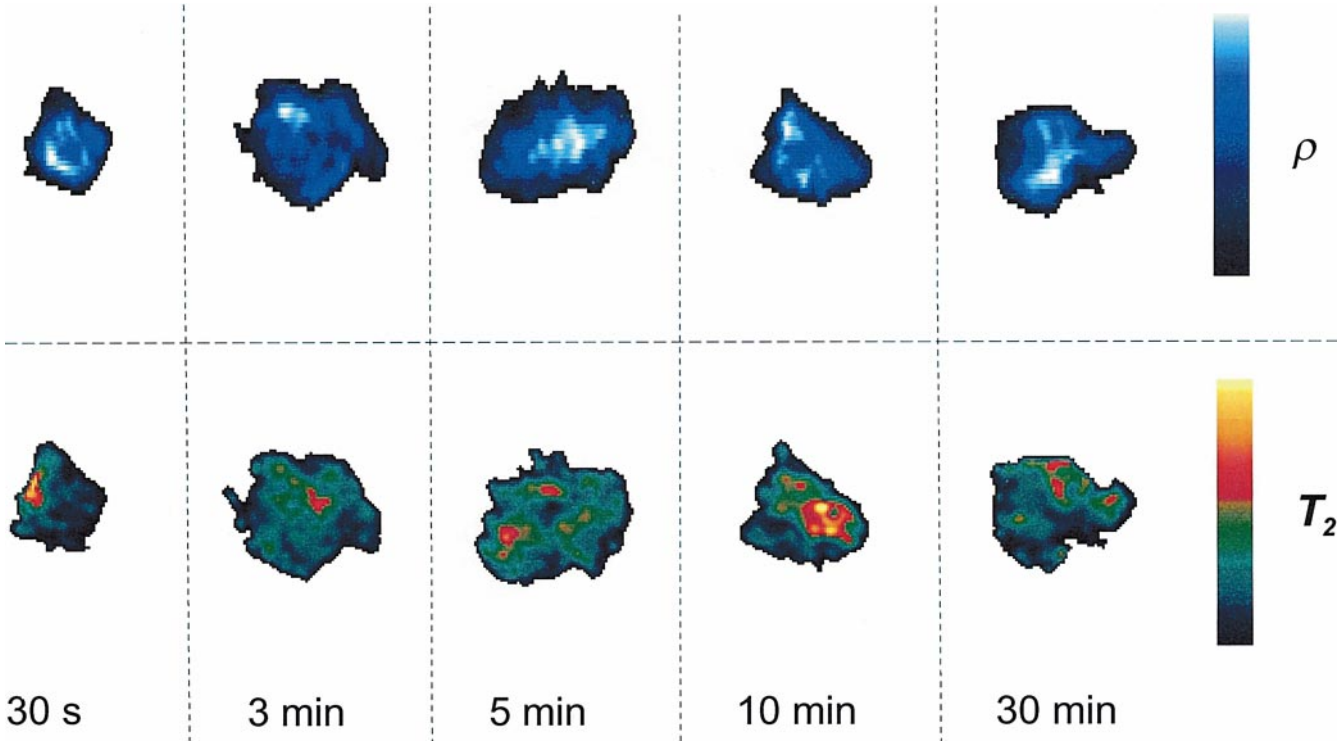

Fig. 5 Spin-density images (*upper part*) and T_2 images (*lower part*) for the five swelling times indicated. Most of the swelling occurs within the first 3 min (note that the orientation of the sample with respect to the imaging plane is different for different swelling times). The *color scale* for T_2 represents values 0–60 ms, while the spin-density scale is given in arbitrary units

imaging. For the acquisition of the image under spinning conditions, a conventional spin-echo back-projection sequence was used, however, with rotating gradients as described in Refs. [16–18]. The gradient strength was 5 G/cm, resulting in a resolution of 600–800 μm. The spin-echo time was set to be 20 ms or more in these experiments, so the signal from the polymer was completely filtered out, i.e., only the contribution of the water was acquired under these conditions.

The resulting image obtained at a rotational frequency of 3 kHz is shown in Fig. 6a. In the middle of the sample a hole can be recognized; this results from the centrifugal force. As a second consequence of the centrifugal force, the spin density in the ring around the hole is found to vary in a radial direction. It increases towards the edge of the sample as is easily visible if one selects a line along the diameter of the image (Fig. 6b). There is practically no signal in the middle (the cutoff intensity was 10% of the maximum intensity), while at around 1.2 mm from the center the signal immediately increases up to about three-quarters of the maximum signal. This distance certainly defines the border of the SAP, which is visible only indirectly in the profile because of the absorbed water. This water must be comparatively strongly adsorbed since, otherwise, it would be driven towards the wall of the rotor (see discussion later). The assumption of such a strongly absorbed water component is supported by 2D nuclear Overhauser enhancement spectroscopy measurements of superabsorbing hydrogels with low degrees of hydration [19].

After being constant for around 0.5 mm, the water signal then increases further as a function of the radius until it reaches its maximum value at the inner wall of the rotor. This increase can be interpreted as being due to relatively mobile (i.e., loosely bound) water. The radial intensity distribution of this component seems to follow a parabolic function (indicated by dotted lines in Fig. 6b). The curvature of this parabola is a qualitative measure of how strongly the water mobility is influenced by presence of the polymer. More quantitative future measurements comparing different SAP samples might use this parameter as a measure of the strength of water absorption.

Conclusions

The use of NMR microimaging methods for the characterization of polyacrylate-based SAPs was explored. Parameter imaging of absorbed water was found to provide information on structural details of the samples. In particular, the T_2 relaxation time and the self-diffusion coefficient were found to be suitable parameters for this investigation. Images of these two parameters reveal differences in the cross-link density of the outer and inner regions of the samples, although they probe different length scales. While T_2 is sensitive to rotational and translational motions in the nanometer range, the self-diffusion coefficient reflects translational motions in the direction of the applied field gradient in the micron range. Self-diffusion imaging was found to provide detailed information on water immobilization attributed to cross-link density inhomogeneities within the inner region of the sample.

A first investigation of the properties of the samples under mechanical load was also performed by taking advantage of the centrifugal forces in MAS imaging. Relying on a preliminary interpretation of the results, it is found that strongly absorbed water and relatively mobile water can be distinguished. The radial intensity distribution of the latter forms a parabola, which is considerably different from what is expected for free water. Such investigations thus promise to provide a measure of the absorption properties of superabsorbing materials.

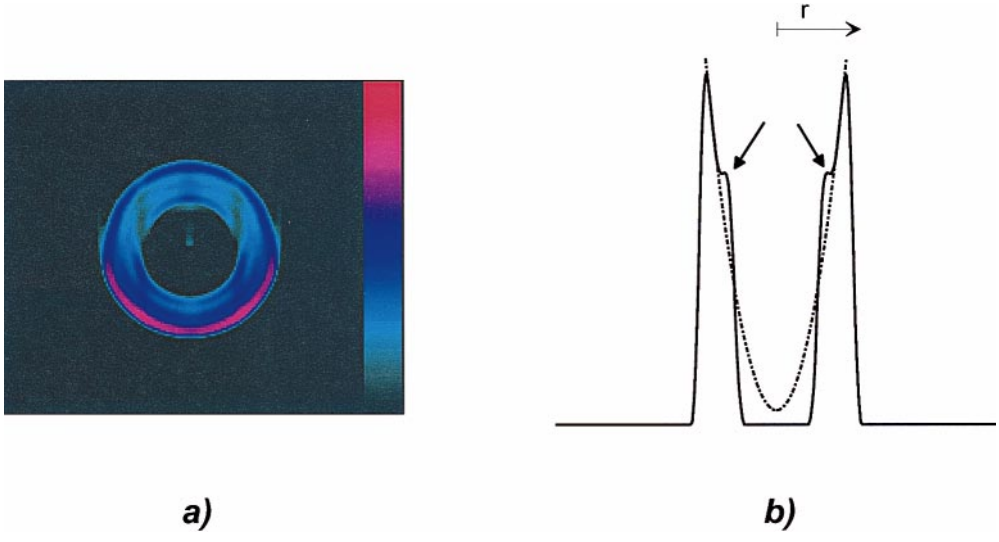

Fig. 6 **a** Back-projection magic-angle-spinning image of a rotor filled with swollen superabsorbing particles. In the *middle* of the image a hole is visible, which results from the centrifugal forces pressing the sample towards the inner wall of the rotor. Within the ring of material, the water density increases radially. **b** Line selected along the diameter of **a** showing the radial distribution of the spin density (i.e., the water density). Following the hole, the spin density is first constant and then increases in the form of a paraboloic function as indicated by the *dotted line*, which is a fit to the data in the outer region. More details are given in the text

Acknowledgements Financial support by the Deutsche Forschungsgemeinschaft is gratefully acknowledged (T.F., S.H.). The authors would also like to thank V. Frenz (BASF AG) for helpful discussions and BASF AG, Ludwigshafen, for providing samples and financial support within the BMBF project (03N6010) ''Innovative Methoden der Polymercharakterisierung für die Praxis'' (BT).

References

1. Namba T, Tsubakimoto T (1994) In: Advances in superabsorbent polymers. American Chemical Society, Washington, DC
2. Morioka K, Nakahigashi S (1992) Refrigeration 618:39
3. Buchholz FL (1994) CHEMTECH 24:38–43
4. Blümler P, Blümich B, Botto R, Fukushima E (eds) (1998) Spatially resolved magnetic resonance Wiley-VCH, Weinheim
5. Miller JB (1998) Prog Nucl Magn Reson Spectrosc 33:273
6. Blümich B, Blümler P (1993) Makromol Chem 194:2133
7. Traub B, Hafner S, Wiesner U, Spiess HW (1998) Macromolecules 31:8585
8. Hafner S NMR Imaging of Polymers In: Meyers R (ed.) (2000) Encyclopedia of analytical chemistry: instrumentation and applications. Wiley, Chichester, in press
9. Webb AG, Hall LD (1991) Polymer 32:2926
10. Grinsted RA, Koenig JL (1992) Macromolecules 25:1229
11. Hafner S, Kuhn W (1994) Magn Reson Imag 12:1075
12. Blümich B (1998) Concepts Magn Reson 10:19
13. Callaghan PT (1991) Principles of nuclear magnetic resonance microscopy. Clarendon, Oxford
14. Kimmich R (1997) NMR tomography, diffusometry and relaxometry. Springer, Berlin Heidelberg New york
15. Stejskal EO, Tanner JE (1965) J Chem Phys 42:288
16. Veeman WS, Cory DG (1989) Adv Magn Reson 13:43
17. Schauss G, Bluemich B, Spiess HW (1991) J Magn Reson 95:437
18. Scheler U, Schauss G, Bluemich B, Spiess HW (1996) Solid State Nucl Magn Reson 6:375
19. Ganapathy S, Rajamohanan PR, Ramanujulu PM, Mandhara AB, Mashelkar RA (1994) Polymer 35:888